PI3-kinase mutation linked to insulin and growth factor resistance in vivo

Jonathon N. Winnay,[1] Marie H. Solheim,[1,2] Ercument Dirice,[1] Masaji Sakaguchi,[1] Hye-Lim Noh,[3] Hee Joon Kang,[3] Hirokazu Takahashi,[1] Kishan K. Chudasama,[2,4] Jason K. Kim,[3] Anders Molven,[2,5,6] C. Ronald Kahn,[1] and Pål R. Njølstad[2,7]

[1]Joslin Diabetes Center, Harvard Medical School, Boston, Massachusetts, USA. [2]KG Jebsen Center for Diabetes Research, Department of Clinical Science, University of Bergen, Bergen, Norway. [3]Division of Endocrinology, Metabolism, and Diabetes, University of Massachusetts Medical School, Worcester, Massachusetts, USA. [4]Department of Cancer Immunology, Institute for Cancer Research, Oslo University Hospital, Oslo, Norway. [5]Gade Laboratory for Pathology, Department of Clinical Medicine, University of Bergen, Bergen, Norway. [6]Department of Pathology and [7]Department of Pediatrics, Haukeland University Hospital, Bergen, Norway.

The phosphatidylinositol 3-kinase (PI3K) signaling pathway is central to the action of insulin and many growth factors. Heterozygous mutations in the gene encoding the p85α regulatory subunit of PI3K (*PIK3R1*) have been identified in patients with SHORT syndrome — a disorder characterized by short stature, partial lipodystrophy, and insulin resistance. Here, we evaluated whether SHORT syndrome–associated *PIK3R1* mutations account for the pathophysiology that underlies the abnormalities by generating knockin mice that are heterozygous for the *Pik3r1*^{Arg649Trp} mutation, which is homologous to the mutation found in the majority of affected individuals. Similar to the patients, mutant mice exhibited a reduction in body weight and length, partial lipodystrophy, and systemic insulin resistance. These derangements were associated with a reduced capacity of insulin and other growth factors to activate PI3K in liver, muscle, and fat; marked insulin resistance in liver and fat of mutation-harboring animals; and insulin resistance in vitro in cells derived from these mice. In addition, mutant mice displayed defective insulin secretion and GLP-1 action on islets in vivo and in vitro. These data demonstrate the ability of this heterozygous mutation to alter PI3K activity in vivo and the central role of PI3K in insulin/growth factor action, adipocyte function, and glucose metabolism.

Introduction

Insulin and most growth factors regulate diverse biological processes, including cell growth, cell survival, and metabolism, by virtue of their ability to activate phosphatidylinositol 3-kinase (PI3K). This leads to generation of phosphatidylinositol 3,4,5 trisphosphate (PIP_3), which in turn activates AKT and other downstream kinases (1). Class 1a PI3Ks exist as obligate heterodimers composed of a regulatory subunit and a catalytic subunit. The regulatory subunits are products of one of 3 genes: PI3K (*PIK3R1*), which gives rise to p85α and its spliced isoforms p55α and p50α; *PIK3R2*, which encodes p85β; and *PIK3R3*, which encodes p55γ. The catalytic subunits are also encoded by 3 genes, *PIK3C1*, *PIK3C2*, and *PIK3C3*, which encode p110α, p110β, and p100γ, respectively. In most somatic tissues, the predominant regulatory and catalytic subunits are p85α and p110α. The fundamental importance of this pathway in insulin action, growth, and metabolism has been demonstrated in studies using pharmacological inhibitors of the enzyme and through the generation of animal models in which genes encoding regulatory or catalytic subunits have been disrupted (2–5). Indeed, homozygous deletion of the genes encoding p110α or p110β or all p85α gene products leads to embryonic or perinatal lethality. Conversely, constitutive activation of this pathway has been linked to the pathogenesis of a variety of cancers and diseases of overgrowth such as Cowden syndrome (6).

SHORT syndrome is an autosomal dominant disorder, which was originally characterized as a condition of short stature, hyperextensibility of the joints and/or hernia, ocular depression, rieger anomaly, and teething delay (7–10). Subsequent evaluation of additional patients revealed other prominent features, including partial lipodystrophy, with a selective reduction in subcutaneous adipose tissue in the face, flank, and buttocks, as well as marked insulin resistance (7, 8). Recently, we and others have shown that the SHORT syndrome is associated with mutations in the *Pik3r1* gene that encodes p85α (11–15). Most mutations cluster in the region encoding the C-terminal SH2 domain of p85α that is essential for binding of PI3K to tyrosine phosphorylated proteins, such as insulin receptor (IR) substrate-1 (IRS-1) and many growth factor receptors (11, 12, 14, 15). The most common mutation in the affected individuals is the Arg649Trp missense mutation; we have demonstrated that this mutation markedly attenuates the insulin-dependent activation of the PI3K pathway in vitro (11). Other missense mutations (Glu489Lys, Arg631Gln), as well as a deletion (Ile539del), truncation (Tyr657*), and frame-shift insertions (Asn636Thrfs*18, Asp643Aspfs*8, Arg649Profs*5), have also been described (3, 7, 8, 15). In the present study, we have generated knockin mice that are heterozygous for the most common mutation (Arg649Trp) observed in patients with SHORT syndrome to define the role of this mutation on the

Authorship note: J.N. Winnay and M.H. Solheim contributed equally to this work. C.R. Kahn and P.R. Njølstad are co-senior authors.
Conflict of interest: The authors have declared that no conflict of interest exists.
Submitted: July 31, 2015; **Accepted:** January 28, 2016.
Reference information: *J Clin Invest*. 2016;126(4):1401–1412. doi:10.1172/JCI84005.

PI3K pathway in vivo and to determine the mechanisms that contribute to the complex phenotype of this disease.

Results

Heterozygosity for the Pik3r1 R649W mutation in mice leads to growth abnormalities. To generate a mouse model of SHORT syndrome that could be used to study the role of the PI3K pathway in insulin action and cell growth in vivo, as well as the pathophysiology of this disease, a synonymous mutation (Arg649Trp or R649W) was introduced into the endogenous *Pik3r1* locus in mice by gene targeting, as described in Supplemental Figure 1A (supplemental material available online with this article; doi:10.1172/JCI84005DS1). Successful introduction of the mutation was confirmed by sequencing genomic DNA from p85α$^{WT/WT}$ and p85α$^{WT/R649W}$ animals (Supplemental Figure 1B). Extensive breeding of p85α$^{WT/R649W}$ mice failed to yield a single homozygous pup, suggesting that homozygosity for the R649W allele results in embryonic lethality. Consistent with clinical features of patients with SHORT syndrome, heterozygous mutant animals exhibited a decrease in size compared with WT littermates (Figure 1A). Growth curves over the first 3 months of life indicated that both male and female p85α$^{WT/R649W}$ mice had significant decreases in body weight when compared with that of controls at all time points examined (Figure 1B). This difference in body weight persisted at 6 months of age, at which time male p85α$^{WT/R649W}$ mice weighed 12.8% less than controls (Figure 1C). Body length was also decreased at 12 weeks of age, with a mean nose-to-anus length of 89.4 ± 2.7 mm compared with 92.8 ± 1.8 mm for controls ($P < 0.01$; Figure 1D), and tibial length was significantly reduced in p85α$^{WT/R649W}$ mice compared with that in controls (16.3 ± 0.08 mm vs. 16.6 ± 0.08 mm, $P < 0.05$; Figure 1E). These changes occurred despite a modest, but significant, elevation in serum IGF-1 levels in p85α$^{WT/R649W}$ mice (12.3 ± 0.17 ng/dl vs. 11.4 ± 0.14 ng/dl, $P < 0.005$; Figure 1F), suggesting the presence of IGF-1 resistance in these animals.

Heterozygous mutant mice exhibit alterations in adipose tissue. Patients with SHORT syndrome exhibit partial lipodystrophy characterized by a selective reduction in subcutaneous adipose tissue (7, 8, 15). Mirroring this phenotype, p85α$^{WT/R649W}$ mice had a significant reduction in subcutaneous adipose tissue mass compared with that of controls (0.66 ± 0.05 g vs. 0.95 ± 0.1 g, $P < 0.05$); this occurred with no change in epididymal white or interscapular brown adipose tissue mass (Figure 2A). This was due to a significant decrease in average adipocyte size in subcutaneous adipose tissue (2,408 ± 29.8 μm^2 vs. 3,039 ± 30.6 μm^2, $P < 0.001$; Figure 2, B and C) and a change in adipocyte size distribution, with a higher frequency of smaller adipocytes (Figure 2, D and E). No change in lean mass was observed, as assessed by dual-energy X-ray absorptiometry analysis. There was also no change in tibialis anterior or liver weight, when adjusted for body weight, indicating proportional growth retardation in other organs of p85α$^{WT/R649W}$ mice (Supplemental Figure 2, A–C). When adjusted for body weight, food and water consumption were unchanged in p85α$^{WT/R649W}$ mice, and exogenous administration of leptin for 72 hours led to a comparable degree of weight loss in control and mutant mice, suggesting that the observed decrease in body size is likely not due to alterations in leptin action (Supplemental Figure 2, D and E). At 9 months of age, there was a significant decrease in epididymal and subcutaneous adipose tissue in mutant animals, and an evaluation of adipocyte area revealed an overall decrease in adipose tissue mass, with a size distribution consistent with a higher frequency of small adipocytes in both depots (Supplemental Figure 2, F–I). In contrast, brown adipose tissue weights, when normalized to body weight, remained unchanged at 9 months of age (Supplemental Figure 2J). Despite these alterations, liver histology as well as circulating free fatty acids and triglycerides remain unaltered in mutant mice (Supplemental Figure 4, A–C). The percentage of adipose tissue progenitor cells isolated from the stromovascular fraction of epididymal and subcutaneous adipose tissue did not differ among the groups (Supplemental Figure 3A). In addition, no change in the differentiation potential of preadipocytes isolated from the stromovascular fraction of subcutaneous and brown adipose tissue was observed between the two groups (Supplemental Figure 3B).

Heterozygous mutant mice are insulin resistant. Most patients with SHORT syndrome are insulin resistant. Although no differences in fasting blood glucose levels were observed (Figure 3A and Supplemental Figure 5A), fed male p85α$^{WT/R649W}$ mice exhibited marked hyperglycemia when compared with controls (318.2 ± 25.3 mg/dl vs. 213.8 ± 15.7 mg/dl, $P < 0.01$; Figure 3A). Fed serum insulin levels were markedly elevated in female p85α$^{WT/R649W}$ mice, whereas both fasted and fed levels were significantly elevated in male p85α$^{WT/R649W}$ mice (Figure 3B and Supplemental Figure 5B), and there was an increase in insulin resistance, as measured by the homeostasis model assessment of insulin resistance (HOMA-IR), which was significantly increased in both male (1.36 ± 0.05 vs. 2.76 ± 0.29, $P < 0.001$) and female (1.29 ± 0.18 vs. 1.88 ± 0.18, $P < 0.05$) mutant mice (Figure 3C and Supplemental Figure 5C). This was associated with a significant elevation of glucose levels during an i.p. glucose tolerance test in both male and female p85α$^{WT/R649W}$ mice compared with that in controls (Figure 3D and Supplemental Figure 5, D and E). Consistent with insulin resistance, both male and female p85α$^{WT/R649W}$ mice showed no decrease in blood glucose during an insulin tolerance test compared with that in controls (Figure 3E and Supplemental Figure 5, F and G). Euglycemic-hyperinsulinemic clamps revealed marked insulin resistance in male p85α$^{WT/R649W}$ mice, with a 58% reduction in the glucose infusion rate when compared with that in controls (46.4 ± 6.63 mg/kg/min vs. 73.3 ± 3.03 mg/kg/min, $P < 0.01$) and a concomitant decrease in the rate of glucose turnover when compared with that in controls (51.8 ± 3.44 mg/kg/min vs. 63.8 ± 2.04 mg/kg/min, $P < 0.05$) (Figure 3G). In addition, hepatic glucose production was only suppressed by 76% in p85α$^{WT/R649W}$ mice compared with 100% suppression in controls, at the concentration of insulin used ($P < 0.01$; Figure 3H). Tissue glucose uptake was evaluated by assessing the uptake of 2-deoxy-[^{14}C] glucose into skeletal muscle, brown fat, and epididymal white adipose tissue following the clamp period. Somewhat surprisingly, no difference was observed in skeletal muscle and brown adipose tissue glucose uptake between WT and mutant mice, but a very significant impairment in glucose uptake in white adipose tissue was observed in p85α$^{WT/R649W}$ mice when compared with that in controls (70.8 ± 12.2 nmol/g/min vs. 32.6 ± 4.2 nmol/g/min; $P < 0.01$; Figure 3I and Supplemental Figure 5H). Oxygen consumption, carbon dioxide production, and respiratory exchange ratio were unaltered in p85α$^{WT/R649W}$ mice when compared with those in controls (Supplemental Figure 6, A and B).

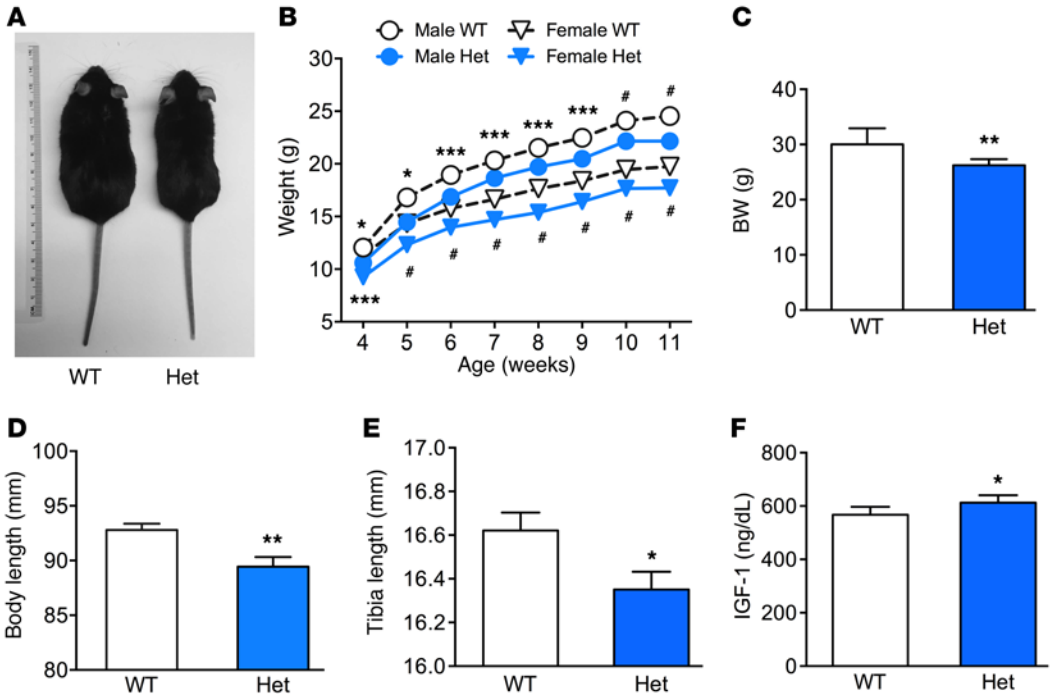

Figure 1. Body weight and length are decreased in p85$^{WT/R649W}$ mice. (**A**) Representative images of female p85α$^{WT/WT}$ (left) and p85α$^{WT/R649W}$ (right) mice at 24 weeks of age. (**B**) Body weight of p85α$^{WT/WT}$ (white) and p85α$^{WT/R649W}$ (red) mice measured over the indicated time course. Female mice are indicated by triangular symbols, and male mice are indicated by circular symbols. (**C**) Body weight at 24 weeks of age and (**D**) body length, (**E**) tibia length, and (**F**) serum IGF-1 levels of 12-week-old male animals. Results are shown as mean ± SEM (n = 9–12). $^{*}P < 0.05$; $^{**}P < 0.01$; $^{***}P < 0.001$; $^{\#}P < 0.0005$, unpaired Student's t test.

Mutant mice exhibit β cell hyperplasia and insulin secretion defect. Previous studies have suggested a role of the PI3K pathway in the regulation of the β cell secretory response (16) as well as generalized effects on cell growth (4). Consistent with systemic insulin resistance, by 12 weeks of age, islets of p85α$^{WT/R649W}$ mice were larger than those of controls upon histological examination (Figure 4A), and quantitation of average islet area revealed a significant 47% increase in islet area in p85α$^{WT/R649W}$ mice compared with that in controls (Figure 4B). On the other hand, secretion of insulin from these islets was defective. Thus, whereas control mice exhibited a 2-fold increase in insulin levels 2 minutes following administration of glucose, this first-phase insulin secretion response was absent in p85α$^{WT/R649W}$ animals (Figure 4C). Furthermore, whereas control islets exhibited a 6.7-fold increase in insulin secretion when transitioned from low to high glucose, islets isolated from mutant animals exhibited elevated basal insulin secretion under low glucose conditions and failed to have an augmented insulin secretory response when transitioned to high glucose (Figure 4D). Furthermore, glucagon-like peptide 1 (GLP-1) treatment of control islets potentiated insulin secretion at both low and high glucose concentrations, while treatment of p85α$^{WT/R649W}$ islets with GLP-1 failed to augment insulin secretion under low glucose conditions and only potentiated secretion in the presence of high glucose concentrations (Figure 4D).

The R649W mutation attenuates IR signaling in vivo. In order to characterize the molecular mechanism(s) contributing to the development of the insulin resistance observed in p85α$^{WT/R649W}$ mice, insulin signaling was assessed in vivo 10 minutes following an insulin injection. Whereas insulin elicited a robust increase in IR phosphorylation in adipose tissue, liver, and skeletal muscle in control animals, this response was significantly attenuated in p85α$^{WT/R649W}$ mice (Supplemental Figure 7A), despite the presence of comparable IR levels (Figure 5A). Likewise, there was a marked decrease in stimulated IRS-1 tyrosine 608 phosphorylation in adipose tissue (89%), liver (37%), and skeletal muscle (83%) from p85α$^{WT/R649W}$ mice (Figure 5A and Supplemental Figure 7B). As predicted, despite the absence of any changes in AKT expression, the insulin-dependent phosphorylation of AKT was also markedly reduced in adipose tissue (63%) and liver (73%) from p85α$^{WT/R649W}$ mice in addition to a more modest, but significant, decrease in skeletal muscle (Figure 5, A and B). This reduction in insulin-dependent phosphorylation of AKT was associated with 72% and 46% reductions in AKT enzyme activity in extracts of liver and skeletal muscle, respectively, from mutant mice (Figure 5C). Immunohistochemistry revealed a robust, insulin-dependent increase in anti-PIP_3 immunoreactivity in livers from p85α$^{WT/WT}$ mice, and this response was visibly diminished in livers from p85α$^{WT/R649W}$ animals (Figure 5D). Consistent with the decrease in AKT phosphorylation/activation, p85α $^{WT/R649W}$ mice also exhibited a decrease in insulin-stimulated phosphorylation of AKT substrates GSK-3α/β and FOXO1/3 in p85α$^{WT/R649W}$ hepatocytes, despite the absence of any change in the expression of the IR, AKT, GSK-3β, or FOXO1 (Figure 5E and Supplemental Figure 8A). Insulin signaling was also assessed in differentiated preadipocytes obtained from subcutaneous adipose tissue of control and mutant mice. In both control and mutant adipocytes, insulin elicited a robust increase in IRS-1 (Y608) and IR phosphorylation (Supplemental Figure 7C). In contrast, whereas

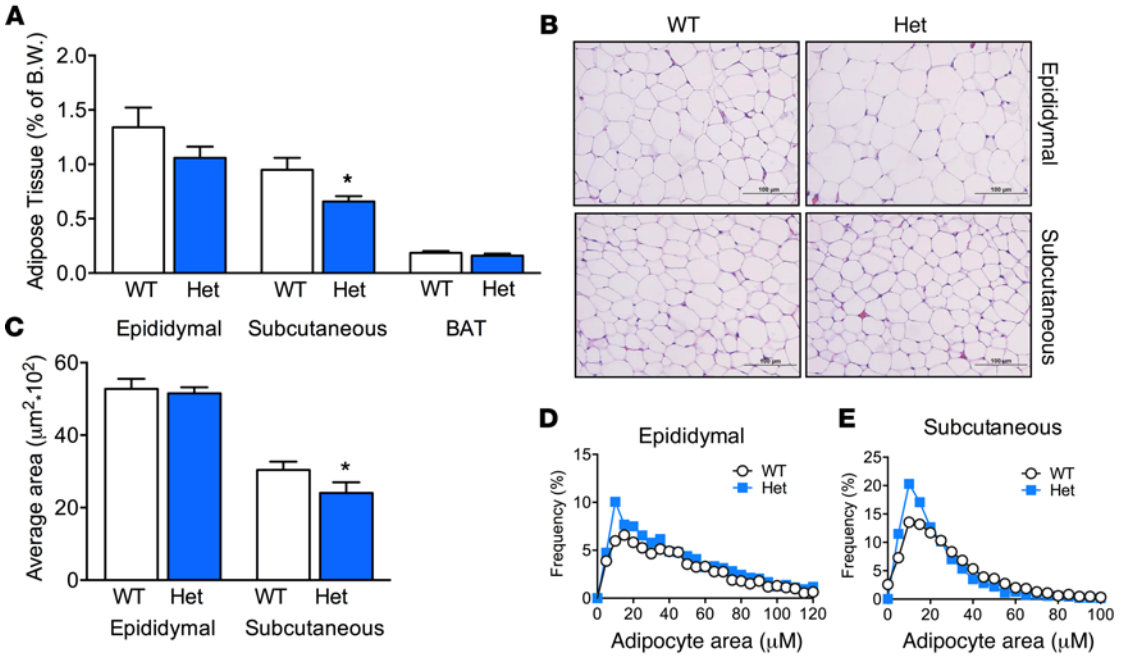

Figure 2. p85$^{WT/R649W}$ mice show a selective reduction in subcutaneous adipose tissue mass. (**A**) Epididymal, subcutaneous, and brown adipose tissue (BAT) expressed as percentage of total body weight in male p85$^{WT/WT}$ and p85$^{WT/R649W}$ mice at 12 weeks of age (n = 9–10). (**B**) Hematoxylin and eosin staining of formalin-fixed tissue sections of epididymal and subcutaneous white adipose tissue (original magnification, ×20). (**C**) Average adipocyte area and distribution of adipocyte size in (**D**) epididymal and (**E**) subcutaneous adipose tissue (n = 3–4). Results are shown as mean ± SEM. *P < 0.05, unpaired Student's t test.

insulin robustly increased AKT (S473/T308) phosphorylation in control cells, this response was attenuated in mutant adipocytes (Supplemental Figure 7C). Collectively, these data demonstrate that the mutant p85α negatively affects the ability of insulin to efficiently activate the PI3K pathway, as well as upstream signaling, in all classical insulin target tissues. The small difference in AKT phosphorylation in skeletal muscle compared with that in other tissues in the knockin mice suggests that other regulatory subunits, such as p85β, may play a larger role in muscle than in other tissues or suggests the presence of some other compensatory pathway in this tissue.

The R649W mutation impairs insulin signaling in vitro. To better understand the multiple effects of the p85α mutation on insulin signaling, immortalized brown preadipocyte cell lines were derived from p85α$^{WT/WT}$ and p85α$^{WT/R649W}$ mice and were stimulated with insulin over a 30-minute time course. Whereas stimulation of p85α$^{WT/WT}$ cells resulted in a robust, time-dependent increase in IRS-1 and AKT phosphorylation, stimulation of p85α $^{WT/R649W}$ cells elicited only a modest increase in phosphorylation of both IRS-1 and AKT (Figure 6A). Likewise, PI3K activity assessed in anti–IRS-1 and anti-phosphotyrosine immunoprecipitates revealed a strong, insulin-dependent increase in p85α$^{WT/WT}$ cells, whereas no increase was observed in p85α$^{WT/R649W}$ cells (Figure 6B). This occurred with no change in the expression of p85α, p110α, and AKT.

In both patients and the knockin mice, the mutant p85α occurs in the presence of one normal p85α allele, as well as other potential regulatory subunits, such as p85β. To examine the signaling capacity of the mutant protein in the absence of endogenous p85α or p85β, we stably transfected immortalized mouse embryonic fibroblasts made from mice with genetic deletion of both *Pik3r1* and *Pik3r2* (and therefore devoid of p85α and p85β) with either WT or R649W p85α. Anti–pan p85 immunoblots confirmed the absence of p85α and p85β in control cells and the reconstitution of comparable levels of the WT or mutant p85α protein (Figure 6C). Reconstitution with either WT or mutant p85α had no effect on insulin-stimulated IR tyrosine phosphorylation when compared with the pBabe control (Figure 6C), but insulin-stimulated tyrosine 608 phosphorylation of IRS-1 was reduced in R649W mutant cells compared with that in controls (Figure 6C). By contrast, IRS-1 phosphorylation at tyrosine Y895 was augmented in cells which expressed either the WT or mutant p85α protein (Figure 6C). As expected, insulin-stimulated AKT phosphorylation was reduced in cells reconstituted with mutant p85α compared with that in controls (1.2 ± 0.16-fold vs. 3.0 ± 0.16-fold, P < 0.01; Figure 6C and Supplemental Figure 9). All of these changes in signaling occurred in the absence of any change in IR, IRS-1, or AKT levels.

Structural modeling and studies in primary fibroblasts isolated from patients with SHORT syndrome have suggested that the R649W mutation acts by reducing p85α binding to phosphorylated motifs on IRS-1 (7, 17, 18). To assess the interaction directly, we performed coimmunoprecipitation studies on p85α/β-deficient embryonic fibroblasts with enforced expression of WT or mutant p85α. p85α could be readily detected in IRS-1 immunoprecipitates from WT p85α cells following insulin stimulation but was not detected in IRS-1 immunoprecipitates from cells expressing mutant p85α (Figure 6D). The same was true when we immunoblotted for IRS-1 in anti-p85α immunoprecipitates from insulin-stimulated cells (Figure 6D). Similarly, coimmunoprecipitation studies performed on HEK293 cells transiently transfected with empty plasmid or vectors encoding V5-tagged WT p85α or p85α^{R649W} showed a failure of the mutant protein to bind to IRS-1

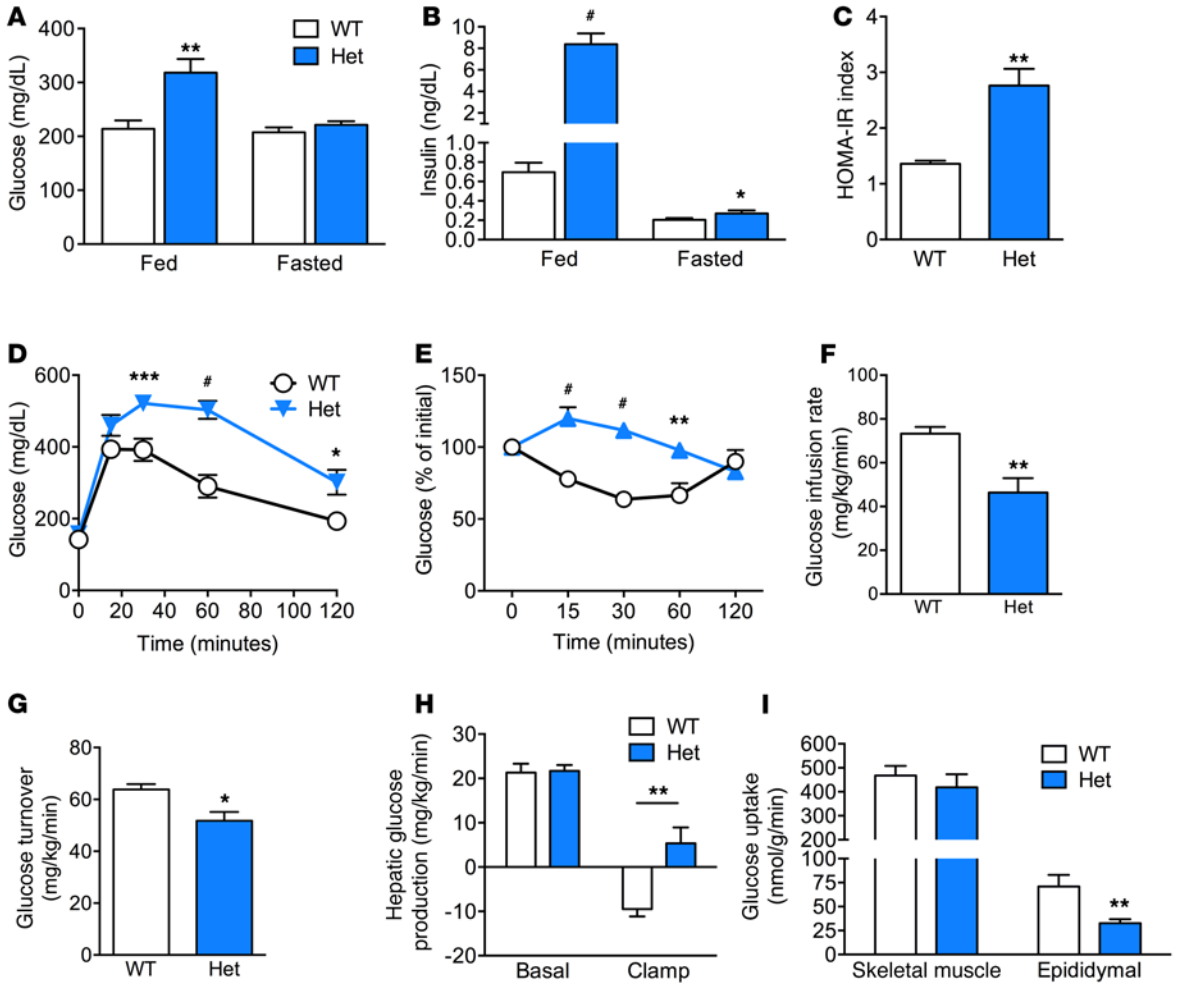

Figure 3. p85$^{WT/R649W}$ mice are glucose intolerant and insulin resistant. (**A**) Blood glucose and (**B**) serum insulin levels in the fasted and fed states in male mice at 8 weeks of age. (**C**) HOMA-IR index calculated using fasting insulin and glucose values. (**D**) Glucose tolerance tests performed at 8 weeks of age in male animals. (**E**) Insulin tolerance tests performed in male mice at 8 weeks of age. (**F**) Glucose infusion rate, (**G**) glucose turnover, and (**H**) hepatic glucose production determined by performing euglycemic/hyperinsulinemic clamps on male mice at 16 weeks of age (n = 7–10). (**I**) Glucose uptake determined from skeletal muscle and epididymal adipose tissue obtained at the end of the clamp period (n = 7–10). Results are expressed as mean ± SEM (n = 9–12 per group). *P < 0.05; **P < 0.01; ***P < 0.001; #P < 0.0005, unpaired Student's t test.

(Supplemental Figure 10). Coimmunoprecipitation studies were also performed to determine whether similar results were obtained in vivo. Although IRS-1 could be readily observed in p85α immunoprecipitates from the livers of WT mice following insulin treatment, p85α failed to precipitate IRS-1 in insulin-stimulated mutant livers (Figure 6E). Thus, the single R649W point mutation in the C-terminal SH2 domain of p85α prevented the formation of the p85α/IRS-1 complex both in vitro and in vivo.

The R649W mutation confers resistance to growth factors. To determine whether the mutation would impair activation of the PI3K pathway downstream of growth factors other than insulin, p85-deficient cells reconstituted with WT or mutant p85α were stimulated with insulin, PDGF, or EGF, and the extent of AKT phosphorylation was assessed. As noted in this and our previous study (11), expression of WT, but not mutant, p85α increased the insulin-dependent phosphorylation of AKT when compared with the control transfected cells (Figure 7A). Similarly, cells expressing WT p85α elicited a very robust increase in PDGF-dependent activation of AKT, which was reduced by >80% in cells expressing the mutant p85α. A modest decrease in AKT activation in cells expressing mutant p85α was also observed with EGF, although overall responsiveness to EGF was low in these cells (Figure 7A). Immunoblots performed with anti-actin antibodies confirmed equal protein loading under all conditions (Supplemental Figure 8B). Likewise, AKT phosphorylation in livers from p85α$^{WT/R649W}$ mice following exogenous administration of EGF was reduced compared with that in controls (Figure 7B and Supplemental Figure 11).

When the PI3K pathway was assessed in isolated hepatocytes from p85α$^{WT/WT}$ and p85α$^{WT/R649W}$ mice, stimulation of AKT phosphorylation by insulin, IGF-1, and EGF was reduced by >50% in p85α$^{WT/R649W}$ hepatocytes compared with that in controls, with no change in the level of receptor activation (Figure 7C). This resulted in a decrease in GSK-3α/β and FOXO1/3a phosphorylation in response to all 3 ligands, with no alteration in the expression of these proteins (Figure 7C and Supplemental Figure 8C). By

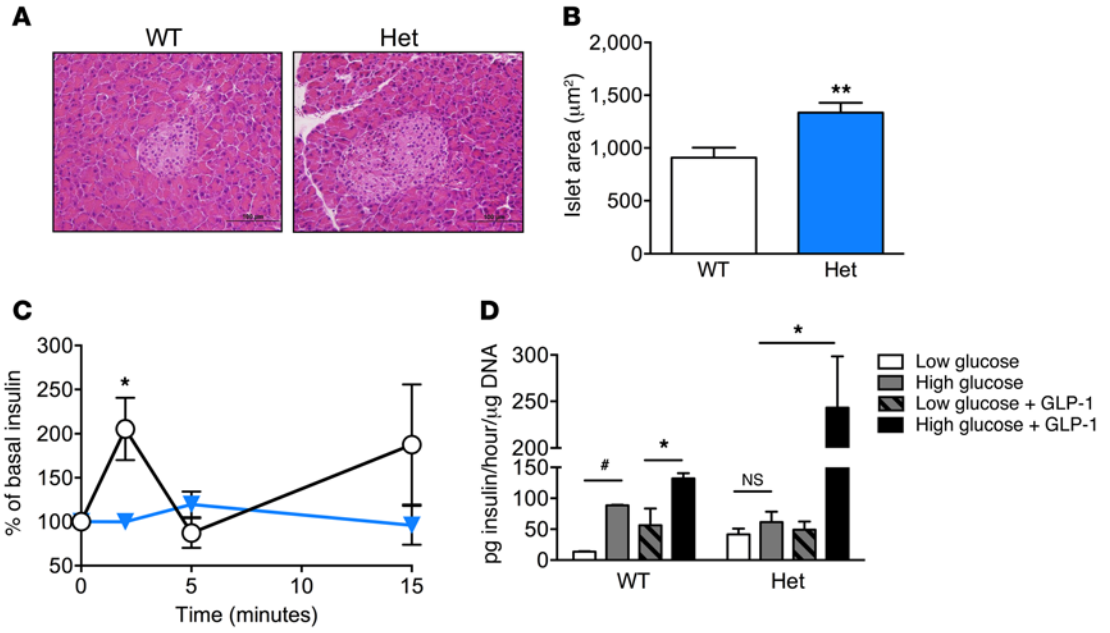

Figure 4. p85$^{WT/R649W}$ mice exhibit islet hyperplasia and an insulin secretory defect. (**A**) Sections of whole pancreas stained with hematoxylin and eosin to visualize islets (original magnification, ×40). (**B**) Measurement of average islet area evaluated using ImageJ (n = 4). (**C**) Glucose-stimulated insulin secretion evaluated in 12-week-old male animals (n = 5). (**D**) Glucose-stimulated insulin secretion assessed in isolated islets from 10-week-old male mice in the absence and presence of GLP-1 (20 ng/dl) (n = 4). Results are expressed as mean ± SEM. *P < 0.05; **P < 0.01; $^{\#}P$ < 0.0005, unpaired Student's t test.

contrast, evaluation of ERK phosphorylation revealed a normal response to insulin and growth factors in mutant cells, indicating that the R649W mutation specifically impairs activation of the PI3K pathway.

Discussion

Although SHORT syndrome is a rare disease, it provides a unique opportunity to define the role of PI3K in human metabolism and growth. In the current study, we have generated mice heterozygous for the *Pik3r1* R649W mutation, the most common mutation in SHORT syndrome, to explore the role of PI3K pathways in insulin action, physiology, and development in vivo. Mutant animals recapitulate many of the features of SHORT syndrome, including reduced body weight and length, reduced subcutaneous adipose tissue mass, alterations in glucose metabolism, and eye abnormalities (the latter will be reported separately). Moreover, using cell lines derived from this mouse and other in vitro models, we demonstrate that this single amino acid mutation in one SH2 domain of p85α, even in a heterozygous form, can impair the ability of insulin and other growth factors to activate the PI3K pathway and exert their downstream effects. This occurs through a loss of p85α binding to phosphorylated motifs on IR substrates and, in the same manner, to the phosphorylated motifs on growth factor receptors. Thus, this mutation negatively affects a variety of processes dependent upon insulin and growth factor action.

One interesting and unexpected aspect of the pathogenesis of this disease is that mice carrying the mutant p85α allele, even in a heterozygous form, are severely insulin resistant, with markedly decreased insulin activation of the PI3K pathway in insulin-responsive tissues, especially liver and adipose tissue. This occurs despite the presence of other PI3K regulatory subunits, such as p85β and p55γ (also known as p55^{PIK}). This is different from the phenotype of mice with a loss of one p85α allele, which demonstrate improved insulin signaling and glucose homeostasis and are protected from the development of diabetes when challenged with high-fat diet or bred to mice with genetic insulin resistance (19–21). The cause of this paradoxical increase in insulin sensitivity in heterozygous p85α-null mice and cells is the unusual stoichiometry of p85α and p110α/β catalytic subunits in normal cells. p85α is in excess of p110α, such that p85α exists as both monomeric (not p110-bound) and dimeric (p110-bound) forms. In p85α heterozygous knockout mice, there is a decrease in monomeric p85α, with only a slight decrease in the amount of p85α/p110 dimer, thereby creating a stoichiometric relationship that favors recruitment of the holoenzyme to IRS-1, leading to enhanced enzymatic activity (22). Likewise, overexpression of p85α in skeletal muscle increases the amount of monomeric p85α, leading to a reduction in insulin action and profound insulin resistance (23). The fact that the heterozygous p85α R649W mice do not phenocopy animals with a reduction in p85α levels indicates that the mutant protein is not simply inactive but is acting in a dominant-negative fashion.

Another unexpected finding in our studies is that the R649W p85α mutant protein also caused defects in signaling upstream of PI3K. In the case of insulin action, this manifested as a significant impairment in IR and IRS-1 tyrosine phosphorylation, which was observed in the knockin mouse in vivo and in some cell lines in vitro. While the exact mechanism of these upstream effects is unknown, several potential mechanisms exist, including changes in the activity of tyrosine phosphatases that dephosphorylate and inactivate the receptor and its substrates, such as protein tyrosine phosphatase 1B (PTP1B) and the LAR phosphatase (24, 25), or changes in subcellular localization or intracellular trafficking of

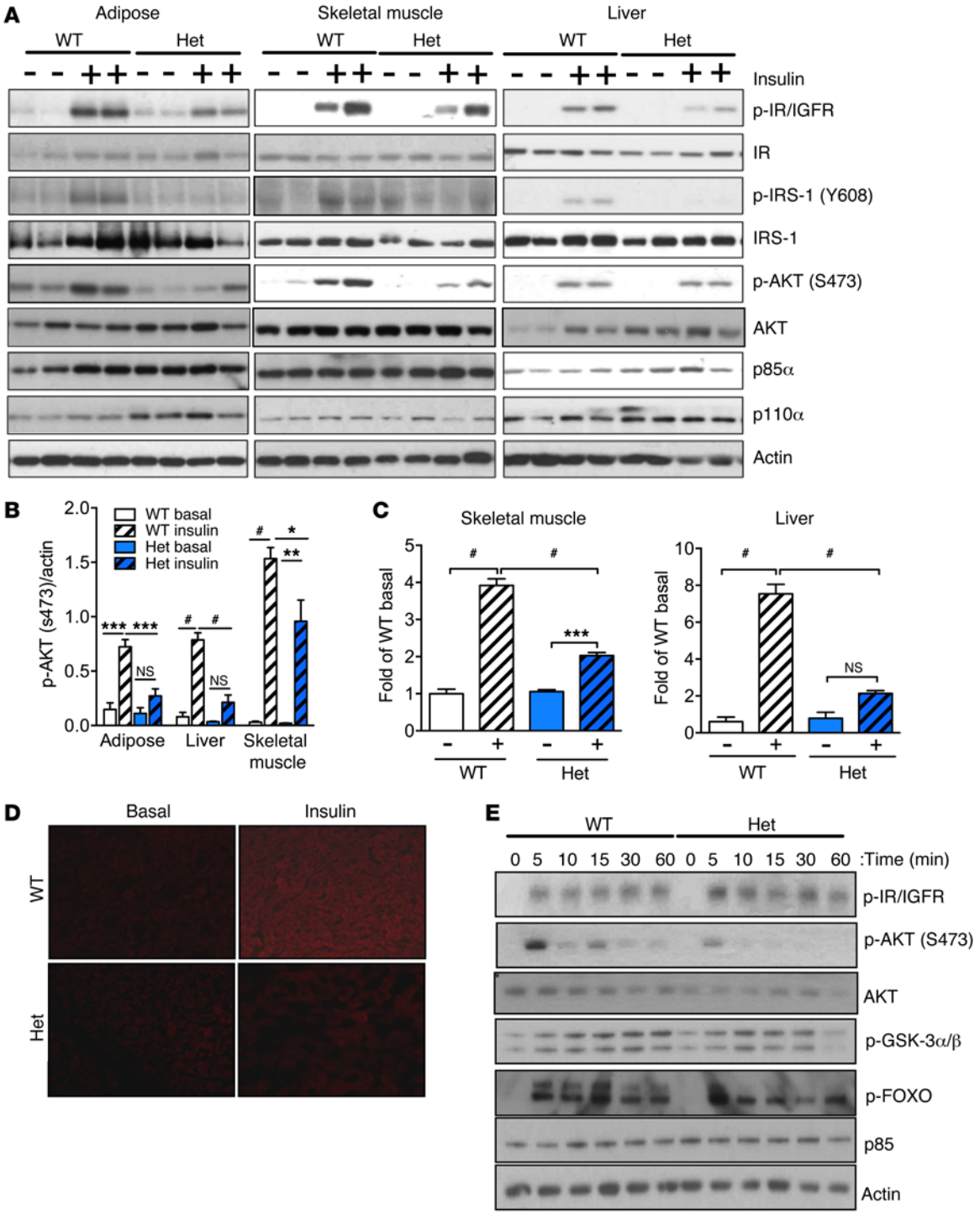

Figure 5. p85$^{WT/R649W}$ mice display impaired insulin signaling in vivo. (**A**) Analysis of insulin signaling in adipose tissue, liver, and skeletal muscle of p85$^{WT/WT}$ and p85$^{WT/R649W}$ mice administered insulin (5 U) or vehicle. Immunoblot analysis was performed with the indicated antibodies. (**B**) Quantification of p-AKT (S473) performed using ImageJ. Results are presented as mean ± SEM (n = 5–6 animals). (**C**) AKT activity was assessed in skeletal muscle and liver (n = 4–5 animals). (**D**) Immunofluorescence performed on liver sections using anti-PIP$_3$ antibody (original magnification, ×40). (**E**) Immunoblot analysis of insulin signaling in primary hepatocytes isolated from p85$^{WT/WT}$ and p85$^{WT/R649W}$ mice in the absence or presence of insulin (10 nM) for the indicated times (n = 3). *P < 0.05; **P < 0.01; ***P < 0.001; #P < 0.0005, unpaired Student's t test.

these proteins mediated by changes in PI3K activity. Alternatively, the sustained hyperinsulinemia observed in mutant animals may lead to receptor desensitization and a concomitant decrease in insulin action, which we observed in vivo in insulin-responsive tissues (26–28). The decrease in the insulin-dependent phosphorylation of tyrosine 608 in IRS-1 that normally mediates binding of p85α may also reflect the fact that the mutant protein cannot bind to this site, leaving it more accessible to phosphotyrosine phos-

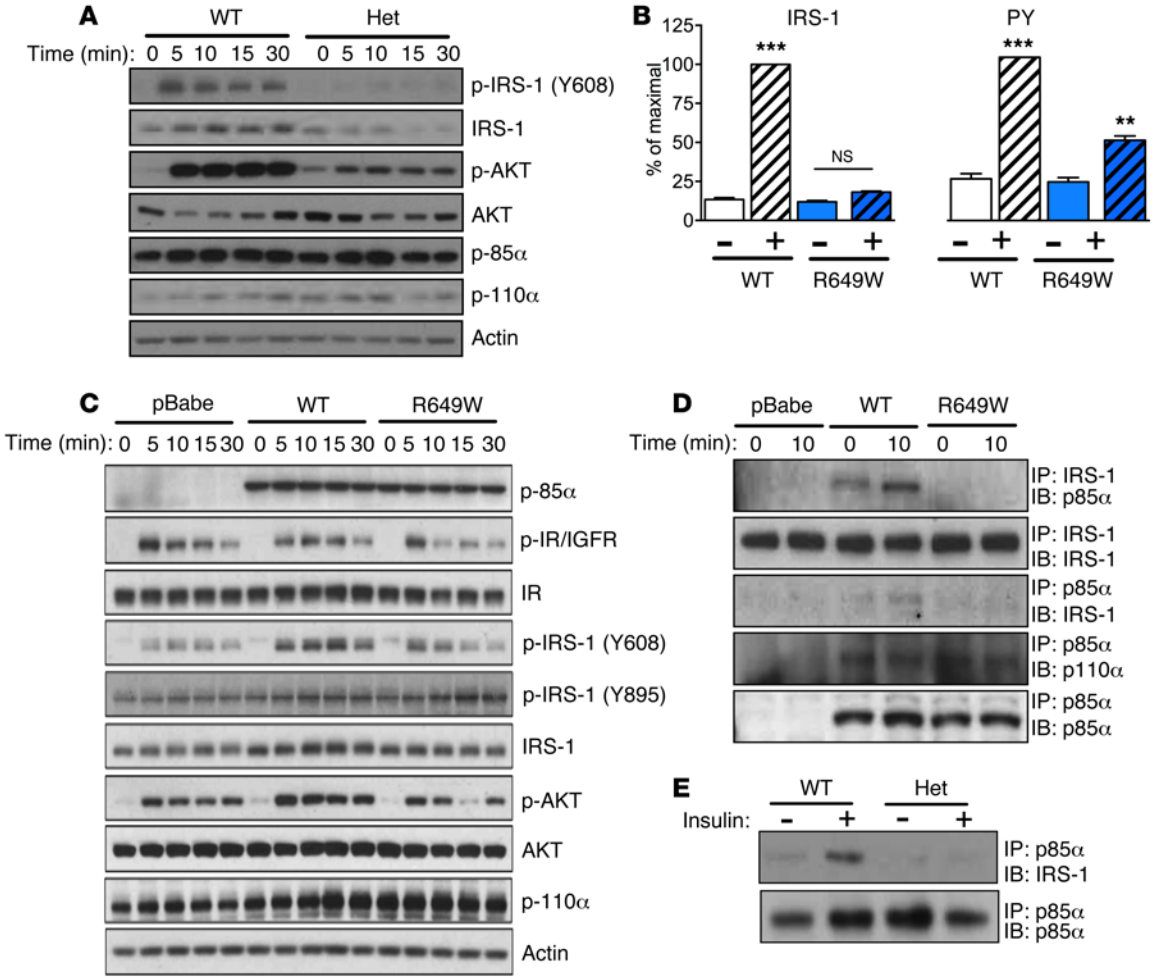

Figure 6. The p85 R649W mutant shows reduced PI3K pathway activation. (**A**) Insulin signaling in brown preadipocytes derived from $p85\alpha^{WT/WT}$ and $p85\alpha^{WT/R649W}$ mice. Cells were treated with insulin (10 nM) over a 30-minute time course. Insulin signaling was analyzed by immunoblotting ($n = 3$). (**B**) Quantification of PI3K assay measuring IRS-1-PI3K activity and PY-PI3K activity in arbitrary optical units in brown preadipocytes derived from $p85\alpha^{WT/WT}$ and $p85\alpha^{WT/R649W}$ mice. Results are presented as mean ± SEM. $^{**}P < 0.01$; $^{***}P < 0.001$, unpaired Student's *t* test. Cumulative data and statistical analysis of 3 independent experiments are presented ($n = 3$). (**C**) PI3K signaling assessed in reconstituted WT and R649W mutant immortalized mouse embryonic fibroblasts void of endogenous p85α/β ($n = 3$). pBabe was used as a control. (**D**) IRS-1 and p85 interaction assessed in p85α/p85β-deficient mouse embryonic fibroblasts reconstituted with WT or R649W mutant p85 ($n = 2$). (**E**) IRS-1 and p85 interaction assessed by coimmunoprecipitation performed in liver lysates from $p85\alpha^{WT/WT}$ and $p85\alpha^{WT/R649W}$ mice ($n = 3$).

phatases (7, 17). In agreement with this hypothesis, the decrease in phosphorylation of IRS-1 was specific to tyrosine 608, which is involved in p85α binding, while the phosphorylation state of tyrosine 895, which binds growth factor receptor–bound protein 2 (GRB2), was not diminished in vivo or in cell models.

A variety of growth factors involved in embryonic and postnatal development depend on PI3K for their action (29–32). Mice homozygous for the R649W mutation do not survive fetal life, and mice heterozygous for the R649W mutation exhibit a reduction in body length and tibial length, despite slightly increased IGF-1 levels, consistent with IGF-1 resistance. Humans with IGF-1 resistance due to IGF-1 receptor mutations exhibit intrauterine and postnatal growth defects and share some features with patients with SHORT syndrome, such as a growth deficit and craniofacial defects, including a triangular face and abnormal size and positioning of the ears (33, 34). Consistent with this hypothesis, growth hormone therapy in patients with SHORT syndrome has largely failed, most likely the result of a significant impairment in the IGF-1 axis.

Activation of the PI3K pathway is required for normal adipogenesis and insulin-dependent regulation of adipocyte metabolism (35–37). Although insulin is required for completion of the normal adipogenic program, we observed no difference in the frequency of adipocyte progenitor cells or the differentiation capacity of preadipocytes isolated from mutant animals. It is possible that the residual activation of the PI3K pathway in mutant cells is sufficient to effectively promote differentiation or the action of other growth factors that facilitate differentiation is not perturbed to a similar degree. Mice with the heterozygous R649W p85α mutation exhibit a reduction in adipose fat mass, primarily due to a reduction in adipocyte size. This is similar to that in mice with a fat-specific IR knockout (38). Missense mutations in *AKT2*, which is downstream of PI3K, lead to severe insulin resistance and partial lipodystrophy in humans (39). Multiple mechanisms are likely involved in these

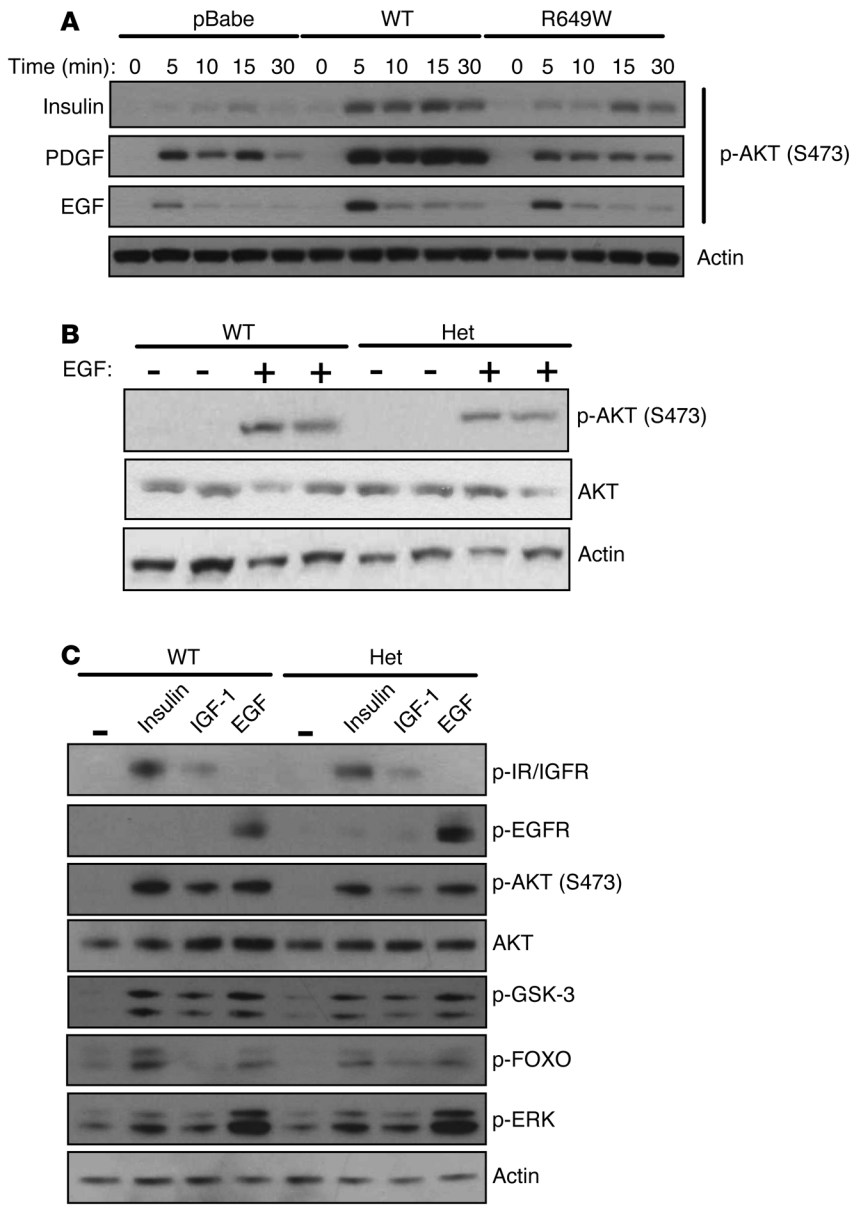

Figure 7. The R649W mutant confers resistance to several growth factors. (**A**) AKT phosphorylation assessed in reconstituted WT and R649W mutant immortalized mouse embryonic fibroblasts treated with insulin, PDGF, and EGF for the indicated time course (n = 2). pBabe was used as a control. (**B**) Analysis AKT phosphorylation in livers of $p85^{WT/WT}$ and $p85^{WT/R649W}$ mice after administration of EGF (1 μg/g body weight) or vehicle for 5 minutes (n = 4–5). (**C**) Signaling in isolated primary hepatocytes following stimulation with insulin, IGF-1, and EGF for 10 minutes (n = 3). Immunoblotting was performed with the indicated antibodies.

various lipodystrophies. Insulin is required for the stimulation of de novo lipogenesis and suppression of lipolysis in adipocytes. Given the degree of insulin resistance observed in adipose tissue from mutant mice, it is likely that the balance between lipid synthesis and lipid metabolism would favor a reduction in the steady-state storage of lipids, leading to an overall reduction in adipocyte size. Insulin is known to stimulate the phosphorylation of lamin A/C via an AKT-dependent mechanism, and mutations of lamin A/C, and this phosphorylation site in particular, are associated with lipodystrophies (40–42).

The deletion of p85α, but not p85β, in the β cell has been shown to lead to impaired first-phase insulin secretion in vivo (16). Similarly, we have observed an insulin secretory defect in mutant mice, highlighting the importance of p85α-mediated signaling in glucose-coupled insulin secretion. Interestingly, although GLP-1 was able to potentiate insulin secretion in control islets, GLP-1 stimulation failed to augment insulin secretion in mutant islets at low glucose but significantly potentiated insulin secretion in high glucose conditions. GLP-1 stimulation has been demonstrated to lead to the acute stimulation of IRS-2 tyrosine phosphorylation and the subsequent recruitment of p85α as well as the p85α-dependent activation of Rap (43, 44). These data suggest that additional therapeutic modalities that augment insulin secretion in addition to insulin therapy may be warranted in patients with SHORT syndrome.

In conclusion, we have generated a mouse model of SHORT syndrome to investigate the pathophysiology of this disease and study the role of the PI3K pathway in vivo in biological processes, such as intrauterine and postnatal growth, development, and metabolism. These mice recapitulate multiple aspects of the disease, including reduced growth, a selective reduction in subcutaneous adipose tissue and the development of insulin resistance, and type 2 diabetes. More importantly, these mice present a clear in vivo demonstration of the role of PI3K in response to insulin as well as several growth factors, including IGF-1, PDGF, and EGF. These data provide mechanistic insight into the physiological role of the PI3K pathway in development and metabolism and demonstrate that the myriad of traits observed in patients with SHORT syndrome represent a state of generalized growth factor resistance.

Methods

Antibodies. Rabbit antibodies specific for phospho-IR/IGFR (product 3024), phospho-AKT (product 4060), pan AKT (product 4691), phospho-GSK-3α/β (product 8566), phospho-IRS-1 Y895 (product 3070) p110α (product 4255), p-FOXO1/FOXO3a (product 9464), GSK-3β (product 9315), and FOXO1 (product 2880) were from Cell Signaling Technology. Phospho-IRS-1 Y608 (catalog 09-432) and p85 (catalog ABS233) antibodies were from EMD Millipore, and antibodies for IR (sc-711), IRS-1 (sc-559), phospho-tyrosine (sc-508), and actin (sc-1616) were from Santa Cruz Biotechnology.

Generation of knockin mouse model with the Pik3r1 R649W mutation. Construction of the targeting vector and generation of the $p85\alpha^{WT/R649W}$ mice was performed by GenOway. Briefly, the genomic

region encompassing exon 17 was amplified by PCR and cloned into the pCR4-TOPO vector (Invitrogen). PCR-based site-directed mutagenesis was performed to introduce the mutation, and the insert was transferred into the targeting vector (CHU1-HR) containing a neomycin selection cassette flanked by FRT sites and loxP sites flanking exon 17 containing the R649W mutation (Supplemental Figure 1A). All exons and PCR fragments used for constructing the targeting vector were validated by DNA sequencing. The targeting vector was electroporated into C57Bl/6 ES cells, and G418-resistant clones were harvested and screened by PCR and Southern blot analysis. The recombined ES cell clones were injected into C57BL/6J blastocysts and were implanted into pseudopregnant females. *PIK3R1*-R649W-neo male mice were bred with female mice that express Flp recombinase to remove the selectable marker. Resultant animals were kept on a C57Bl/6J background and housed on a 12-hour-light/12-hour-dark cycle, with ad libitum access to water and food (mouse diet F9; PMI Nutrition International).

Assessment of glucose metabolism. Blood glucose was measured in whole venous blood in the random fed state or following a 16-hour fast using the Infinity blood glucose monitoring system (USDiagnostic). Insulin levels were determined using an ELISA assay (Crystal Chem). For glucose tolerance testing, mice were fasted overnight (16 hours) and injected intraperitoneally with glucose at a dose of 2 g/kg body weight, and blood glucose concentrations were measured at the indicated time points. Insulin tolerance tests were performed by intraperitoneal administration of insulin (1 U/kg body weight) to mice in the random fed state followed by measurement of blood glucose concentrations at the indicated time points.

Hyperinsulinemic-euglycemic clamp and in vivo glucose uptake. The clamp was conducted in overnight-fasted, conscious mice by the National Mouse Metabolic Phenotyping Center at the University of Massachusetts Medical School (45). Briefly, whole-body glucose turnover was assessed using a continuous infusion of [3-^{3}H] glucose, and a bolus injection of 2-deoxy-[^{14}C] glucose was used during the clamp to measure insulin-stimulated glucose uptake in individual organs. Biochemical analysis and calculations were done as previously described (45).

Islet isolation and in vitro insulin secretion assay. Islets were isolated using the intraductal collagenase technique (46). Intact islets were hand picked under a stereomicroscope and allowed to recover overnight. Islets of similar sizes were then further selected, and 20 islets were transferred to each well of a 12-well plate to perform secretion experiments. Islets were preincubated in KRBH buffer supplemented with 2% BSA for 1 hour prior to incubation in low (2.8 mM) or high (16.7 mM) glucose in the presence or absence of GLP-1 (20 ng/ml). After incubation, media were collected, centrifuged, and stored at –20°C for determination of insulin levels by ELISA (Crystal Chem). Islets were collected, and DNA was extracted and quantified to normalize data.

Cell culture and treatment. All cells were cultured in DMEM supplemented with 10% FBS, penicillin, and streptomycin (Thermo Fisher Scientific) at 37°C and 5% CO_2. Before treatment, cells were serum deprived in DMEM supplemented with 0.1% BSA for 3 hours and treated in the absence or presence of insulin, EGF, PDGF, or IGF-1 (Peprotech) for the indicated time points.

Protein extraction and immunoblotting. Cells and tissues were collected and lysed/homogenized in RIPA lysis buffer (EMD Millipore) supplemented with protease and phosphatase inhibitor cocktails (Biotools). Nuclei and insoluble debris were pelleted using a microcentrifuge at 21,130 g for 10 minutes at 4°C. Cells extracts were stored at –80°C or immediately subjected to SDS-PAGE. Protein concentrations were determined using the BCA assay according to the manufacturer's instructions (Thermo Fisher Scientific). Protein lysates were subjected to SDS-PAGE and transferred to PVDF membrane (EMD Millipore). Immunoblotting was performed using the indicated antibodies. Quantification of immunoblots was performed using ImageJ. For immunoprecipitation studies, protein lysates were incubated overnight with the indicated antibodies. Immune complexes were captured by incubation with Protein A/G Plus-Agarose (Santa Cruz Biotechnology) for 1 hour at 4°C, washed 3 times with lysis buffer, and resolved by SDS-PAGE.

PI3K assay. Immunoprecipitations with the indicated antibodies were performed overnight in buffer A containing 25 mM Tris-HCl (pH 7.4), 2 mM Na_3VO_4, 10 mM NaF, 10 mM $Na_4P_2O_7$, 1 mM EGTA, 1 mM EDTA, and 1% Nonidet P-40 supplemented with protease and phosphatase inhibitor cocktails (Biotools). Immune complexes were captured with Protein A/G Plus-Agarose (Santa Cruz Biotechnology) for 1 hour at 4°C. Immunoprecipitates were washed 3 times in buffer A containing 500 mM NaCl and 2 times in PI3K reaction buffer (20 mM Tris-HCl [pH 7.4], 100 mM NaCl, 0.5 mM EGTA) and suspended in 50 μl of PI3K reaction buffer containing 0.1 mg phosphatidylinositol/ml (Avanti Polar Lipids). The reactions were performed for 25 minutes at room temperature, and phosphorylated lipids were separated by thin-layer chromatography (TLC) as previously described (42).

AKT assay. AKT activity was assessed essentially as previously described (47). Briefly, cells were lysed with buffer A supplemented with protease and phosphatase inhibitors, and lysates were subjected to immunoprecipitation with anti-AKT antibodies (Santa Cruz Biotechnology). Immunoprecipitates were washed 3 times with buffer A and once with kinase reaction buffer (50 mM Tris-HCl [pH 7.5], 10 mM $MgCl_2$, and 1 mM dithiothreitol). Immunoprecipitates were resuspended in kinase reaction buffer, to which 50 μM ATP, 5 μCi [γ^{32}P] ATP, and 1 μg peptide substrate was added. Following a 20-minute incubation at 30°C, the reaction was stopped, aliquots were spotted onto P-81 phosphocellulose paper and washed with 0.5% phosphoric acid, and radioactivity was measured.

Isolation of primary hepatocytes. The isolation of primary hepatocytes from WT and p85α$^{WT/R649W}$ animals was achieved as previously described with minor modifications (48). The liver was perfused via the portal vein with liver perfusion media (0.02% EGTA solution buffer) and digested with liver digestion media (Earl's Balanced Salts, 2% penicillin and streptomycin, and 0.4 mg/ml collagenase). The liver was excised, and hepatocytes were released by manual disruption of the tissue. Hepatocytes were then layered on a 90% Percoll gradient and centrifuged at 180 g for 10 minutes. The viable cells were recovered from the bottom of the tube. Cells were seeded onto collagen-coated plates, and the media were changed after 4 hours. Primary hepatocyte experiments were performed the day after isolation.

Histological analysis. Tissues were fixed overnight with neutral-buffered 10% formalin at 4°C, paraffin embedded, sectioned, and stained with hematoxylin and eosin. Adipocyte area was determined by quantifying the adipocyte area of a minimum of 750 cells from 4 to 5 animals per study group using Adiposoft image analysis software.

Statistics. All data are presented as mean ± SEM. GraphPad Prism software (version 6) was used to perform the statistical analysis. Unpaired, 1-tailed *t* tests or 1-way ANOVA (Tukey's multiple compar-

ison test) were used to analyze differences among the control group and one or more independent treatment groups. A *P* value of less than 0.05 was considered significant.

Study approval. All animal experiments were approved by and conducted in accordance with guidelines established by the Institutional Animal Care and Use Committee at the Joslin Diabetes Center.

Author contributions

ED, HT, MS, KKC, HN, HJK, and JKK designed and performed experiments and interpreted data. JNW, MHS, AM, CRK, and PRN oversaw all aspects of this research.

Acknowledgments

We would like to thank Rohit Kulkarni at the Joslin Diabetes Center for helpful discussion. We would like to thank the Physiology Core at the Joslin Diabetes Center for performing and interpreting the comprehensive lab animal monitoring system and dual-energy X-ray absorptiometry analysis and the National Mouse Metabolic Phenotyping Center at the University of Massachusetts Medical School for performing the hyperinsulinemic-euglycemic clamp study. This work was supported by R01 DK055545 (to C.R. Kahn) from the National Institute of Digestive and Diabetes and Kidney Diseases. The National Mouse Metabolic Phenotyping Center at the University of Massachusetts is funded by NIH grant U24-DK093000. This work was also supported by the European Research Council (293574 to P.R. Njølstad), the Research Council of Norway (to P.R. Njølstad), the University of Bergen, and the Western Regional Health Authorities. M.H. Solheim was supported in part by funds from the University of Bergen, the KG Jebsen Foundation, the Norwegian Society of Endocrinology, Eckbo's Foundation, Tom Wilhelmsen Foundation, and the Norwegian Diabetes Association.

Address correspondence to: C. Ronald Kahn, Joslin Diabetes Center, Section on Integrative Physiology and Metabolism, One Joslin Place, Boston, Massachusetts 02215, USA. Phone: 617.732.2635; E-mail: c.ronald.kahn@joslin.harvard.edu. Or to: Pål R. Njølstad, Department of Clinical Science, University of Bergen, Department of Pediatrics, Haukeland University Hospital, N-5021 Bergen, Norway. Phone: 47.55.97.51.53; E-mail: pal.njolstad@uib.no.

1. Vanhaesebroeck B, Stein RC, Waterfield MD. The study of phosphoinositide 3-kinase function. *Cancer Surv*. 1996;27:249–270.
2. Fruman DA, et al. Hypoglycaemia, liver necrosis and perinatal death in mice lacking all isoforms of phosphoinositide 3-kinase p85 alpha. *Nat Genet*. 2000;26(3):379–382.
3. Sharma PM, et al. Inhibition of phosphatidylinositol 3-kinase activity by adenovirus- mediated gene transfer and its effect on insulin action. *J Biol Chem*. 1998;273(29):18528–18537.
4. Cheatham B, Vlahos CJ, Cheatham L, Wang L, Blenis J, Kahn CR. Phosphatidylinositol 3-kinase activation is required for insulin stimulation of pp70 S6 kinase, DNA synthesis, and glucose transporter translocation. *Mol Cell Biol*. 1994;14(7):4902–4911.
5. Bi L, Okabe I, Bernard DJ, Wynshaw-Boris A, Nussbaum RL. Proliferative defect and embryonic lethality in mice homozygous for a deletion in the p110α subunit of phosphoinositide 3-kinase. *J Biol Chem*. 1999;274(16):10963–10968.
6. Liaw D, et al. Germline mutations of the PTEN gene in Cowden disease, an inherited breast and thyroid cancer syndrome. *Nat Genet*. 1997;16(1):64–67.
7. Sorge G, Ruggieri M, Polizzi A, Scuderi A, Di Pietro M. SHORT syndrome: a new case with probable autosomal dominant inheritance. *Am J Med Genet*. 1996;61(2):178–181.
8. Schwingshandl J, Mache CJ, Rath K, Borkenstein MH. SHORT syndrome and insulin resistance. *Am J Med Genet*. 1993;47(6):907–909.
9. Lipson AH, Cowell C, Gorlin RJ. The SHORT syndrome: further delineation and natural history. *J Med Genet*. 1989;26(7):473–475.
10. Aarskog D, Ose L, Pande H, Eide N. Autosomal dominant partial lipodystrophy associated with Rieger anomaly, short stature, and insulinopenic diabetes. *Am J Med Genet*. 1983;15(1):29–38.
11. Chudasama KK, et al. SHORT syndrome with partial lipodystrophy due to impaired phosphatidylinositol 3 kinase signaling. *Am J Hum Genet*. 2013;93(1):150–157.
12. Schroeder C, et al. PIK3R1 mutations in SHORT syndrome. *Clin Genet*. 2014;86(3):292–294.
13. Barcena C, et al. Exome sequencing identifies a novel mutation in PIK3R1 as the cause of SHORT syndrome. *BMC Med Genet*. 2014;15:51.
14. Dyment DA, et al. Mutations in PIK3R1 cause SHORT syndrome. *Am J Hum Genet*. 2013;93(1):158–166.
15. Thauvin-Robinet C, et al. PIK3R1 mutations cause syndromic insulin resistance with lipoatrophy. *Am J Hum Genet*. 2013;93(1):141–149.
16. Kaneko K, et al. Class IA phosphatidylinositol 3-kinase in pancreatic β cells controls insulin secretion by multiple mechanisms. *Cell Metab*. 2010;12(6):619–632.
17. Delahaye L, Mothe-Satney I, Myers MG Jr, White MF, Van Obberghen E. Interaction of insulin receptor substrate-1 (IRS-1) with phosphatidylinositol 3-kinase: effect of substitution of serine for alanine in potential IRS-1 serine phosphorylation sites. *Endocrinology*. 1998;139(12):4911–4919.
18. Rocchi S, Tartare-Deckert S, Mothe I, Van Obberghen E. Identification by mutation of the tyrosine residues in the insulin receptor substrate-1 affecting association with the tyrosine phosphatase 2C and phosphatidylinositol 3-kinase. *Endocrinology*. 1995;136(12):5291–5297.
19. Mauvais-Jarvis F, et al. Reduced expression of the murine p85alpha subunit of phosphoinositide 3-kinase improves insulin signaling and ameliorates diabetes. *J Clin Invest*. 2002;109(1):141–149.
20. Chen D, et al. p50α/p55α phosphoinositide 3-kinase knockout mice exhibit enhanced insulin sensitivity. *Mol Cell Biol*. 2004;24(1):320–329.
21. Ueki K, et al. Increased insulin sensitivity in mice lacking p85beta subunit of phosphoinositide 3-kinase. *Proc Natl Acad Sci U S A*. 2002;99(1):419–424.
22. Ueki K, Fruman DA, Brachmann SM, Tseng YH, Cantley LC, Kahn CR. Molecular balance between the regulatory and catalytic subunits of phosphoinositide 3-kinase regulates cell signaling and survival. *Mol Cell Biol*. 2002;22(3):965–977.
23. Barbour LA, et al. Increased P85α is a potent negative regulator of skeletal muscle insulin signaling and induces in vivo insulin resistance associated with growth hormone excess. *J Biol Chem*. 2005;280(45):37489–37494.
24. Bandyopadhyay D, et al. Protein-tyrosine phosphatase 1B complexes with the insulin receptor in vivo and is tyrosine-phosphorylated in the presence of insulin. *J Biol Chem*. 1997;272(3):1639–1645.
25. Goldstein BJ, Bittner-Kowalczyk A, White MF, Harbeck M. Tyrosine dephosphorylation and deactivation of insulin receptor substrate-1 by protein-tyrosine phosphatase 1B. *J Biol Chem*. 2000;275(6):4283–4289.
26. Soli AH, Kahn CR, Neville DM Jr, Roth J. Insulin receptor deficiency in genetic and acquired obesity. *J Clin Invest*. 1975;56(4):769–780.
27. Goldfine ID, Kahn CR, Neville DM Jr, Roth J, Garrison MM, Bates RW. Decreased binding of insulin to its receptors in rats with hormone induced insulin resistance. *Biochem Biophys Res Commun*. 1973;53(3):852–857.
28. Crettaz M, Kahn CR. Insulin receptor regulation and desensitization in rat hepatoma cells. *Diabetes*. 1984;33(5):477–485.
29. Engelman JA, Luo J, Cantley LC. The evolution of phosphatidylinositol 3-kinases as regulators of growth and metabolism. *Nat Rev Genet*. 2006;7(8):606–619.
30. Baker J, Liu JP, Robertson EJ, Efstratiadis A. Role of insulin-like growth factors in embryonic and postnatal growth. *Cell*. 1993;75(1):73–82.
31. Kruis T, et al. Heterozygous mutation within a kinase-conserved motif of the insulin-like growth factor I receptor causes intrauterine and postnatal growth retardation. *J Clin Endocrinol Metab*. 2010;95(3):1137–1142.
32. Wallborn T, et al. A heterozygous mutation of

the insulin-like growth factor-I receptor causes retention of the nascent protein in the endoplasmic reticulum and results in intrauterine and postnatal growth retardation. *J Clin Endocrinol Metab*. 2010;95(5):2316–2324.
33. Batey L, et al. A novel deletion of IGF1 in a patient with idiopathic short stature provides insight Into IGF1 haploinsufficiency. *J Clin Endocrinol Metab*. 2014;99(1):E153–E159.
34. Fuqua JS, Derr M, Rosenfeld RG, Hwa V. Identification of a novel heterozygous IGF1 splicing mutation in a large kindred with familial short stature. *Horm Res Paediatr*. 2012;78(1):59–66.
35. Tomiyama K, Nakata H, Sasa H, Arimura S, Nishio E, Watanabe Y. Wortmannin, a specific phosphatidylinositol 3-kinase inhibitor, inhibits adipocytic differentiation of 3T3-L1 cells. *Biochem Biophys Res Commun*. 1995;212(1):263–269.
36. Yu W, et al. Critical role of phosphoinositide 3-kinase cascade in adipogenesis of human mesenchymal stem cells. *Mol Cell Biochem*. 2008;310(1–2):11–18.
37. Sakaue H, et al. Posttranscriptional control of adipocyte differentiation through activation of phosphoinositide 3-kinase. *J Biol Chem*. 1998;273(44):28945–28952.
38. Bluher M, et al. Adipose tissue selective insulin receptor knockout protects against obesity and obesity-related glucose intolerance. *Dev Cell*. 2002;3(1):25–38.
39. George S, et al. A family with severe insulin resistance and diabetes due to a mutation in AKT2. *Science*. 2004;304(5675):1325–1328.
40. Cenni V, et al. Lamin A Ser404 is a nuclear target of Akt phosphorylation in C2C12 cells. *J Proteome Res*. 2008;7(11):4727–4735.
41. Marmiroli S, et al. A-type lamins and signaling: the PI 3-kinase/Akt pathway moves forward. *J Cell Physiol*. 2009;220(3):553–561.
42. Ueki K, Algenstaedt P, Mauvais-Jarvis F, Kahn CR. Positive and negative regulation of phosphoinositide 3-kinase-dependent signaling pathways by three different gene products of the p85α regulatory subunit. *Mol Cell Biol*. 2000;20(21):8035–8046.
43. Trumper J, Ross D, Jahr H, Brendel MD, Goke R, Horsch D. The Rap-B-Raf signalling pathway is activated by glucose and glucagon-like peptide-1 in human islet cells. *Diabetologia*. 2005;48(8):1534–1540.
44. Trumper K, Trumper A, Trusheim H, Arnold R, Goke B, Horsch D. Integrative mitogenic role of protein kinase B/Akt in β-cells. *Ann N Y Acad Sci*. 2000;921:242–250.
45. Kim JK. Hyperinsulinemic-euglycemic clamp to assess insulin sensitivity in vivo. *Methods Mol Biol*. 2009;560:221–238.
46. Kulkarni RN, et al. Leptin rapidly suppresses insulin release from insulinoma cells, rat and human islets and, in vivo, in mice. *J Clin Invest*. 1997;100(11):2729–2736.
47. Ueki K, et al. Potential role of protein kinase B in insulin-induced glucose transport, glycogen synthesis, and protein synthesis. *J Biol Chem*. 1998;273(9):5315–5322.
48. Jelen S, et al. Aquaporin-9 protein is the primary route of hepatocyte glycerol uptake for glycerol gluconeogenesis in mice. *J Biol Chem*. 2011;286(52):44319–44325.